COMPUTATIONAL STUDY ON THE EFFECTS OF TURBULENCE INTENSITY AND PULSE FREQUENCY IN SOOT AND NO_X EMISSIONS IN GASEOUS DIFFUSION FLAMES

Fernando Lopez-Parra
General Electric Company Polska

Abstract

The main objective of the work presented in this paper will be to present and discuss the development and implementation of a numerical model to simulate soot formation and depletion in turbulent diffusion flames. The relevance of such model lays on the importance of tying the formation of soot to the ongoing reaction mechanism so that it is fully integrated into the combustion process. The model presented is capable of taking into account the direct effects of turbulence on the amount of soot that is produced in non-premixed flames.

This research focuses on the study of an axi-symmetric C_2H_2 – air turbulent diffusion flame issued from a 3mm round jet with Reynolds number values between 8000 and 16500. The trend observed in the net production of soot with respect to the turbulence intensity is in good agreement with the empirical results found in the literature. These reveal a decrease in soot formation with increasing turbulence. This interaction between particulates and turbulence was then exploited in order to develop a mechanical technique by which a simultaneous reduction in soot and NO_x was achieved.

The level of turbulence was increased locally by application of a sinusoidal pulse frequency to the fuel stream. Such technique reduced the size of the soot-prone, fuel-rich region, with respect to the equivalent steady state flame, by means of enhancing the mixing between the fuel and the oxidizer.

The Realizable k-ε model was employed to solve the turbulence transport, whereas the reaction was simulated with a 1-reaction step mechanism and the turbulence-chemistry interaction was solved using the Eddy Dissipation Model. The size of the time steps employed in the unsteady configuration for pulsed flames was $1/20^{th}$ of the pulse period.

The soot model employed in this work observed two different stages in the soot formation process: nuclei inception and particle growth. As a result two transport equations are solved mass fractions of nuclei and soot respectively. The implementation of this model is achieved through user-defined functions that supersede the source terms in the default soot transport equations. Furthermore, the production of NO_x was simulated using a classic Zel'dovich mechanism with partial equilibrium assumption for release of atomic oxygen, O, and hydroxyl groups, OH.

1. INTRODUCTION

The task of reducing soot emissions through fuel stream excitation can be a tedious process unless a design guideline for the pulse shape and sequencing can be defined.

Employing a pair of frequencies with incommensurate periods in a non-linear system generates a diverse range of fluctuations, effectively increasing the number of pulses affecting the system. The latter will respond to those that are closer to system resonance frequency.

The emission of combustion-derived pollutants is an area of major interest due to the strong environmental impact caused by the unwanted products of reaction. Although the appearance of most pollutant species might not depend on fuel or flame configuration, the relative concentration of these species varies with different flame generation processes and environmental conditions. In diesel combustion engines and, in general, any non-premixed hydrocarbon combustion process, soot forms one of the primary pollutant emissions. In spite of the mechanisms of soot formation not being completely agreed upon universally nowadays, the behaviour of this carcinogenic specie [1],[2] has been computationally reproduced with an acceptable degree of accuracy since the early days of combustion simulation [3-10].

Soot particulates are formed in the fuel-rich zones of the flame, where the breakdown of the fuel molecules (pyrolysis) occurs. In some cases, the entrained oxygen does not reach these molecules and they form highly reactive carbon radicals. It is universally accepted that nucleation, surface growth and agglomeration is the sequence in which soot particulates are formed. An important part of the soot formed is then burnt in the stoichiometric and fuel-lean regions of the flame, where high temperatures and higher concentrations of oxygen are found.

In recent decades, a diversity of soot models have been implemented in either in-house or commercial computational fluid dynamics (CFD) solvers. Some of these soot models, especially those developed in the early stages of soot simulation, were based on mathematical relationships deduced from empirical observations [8, 9, 11]. As the mechanisms of soot production were investigated, the importance of soot formation in the evolution of the flame has been pinpointed. The main part of this interference of soot with the flame resides in the energy balance, since soot absorbs a considerable amount of the heat produced in the combustion and tends to transfer it to the surrounding walls through radiation, as seen in furnace applications, for example. For this reason it is of utmost importance to simulate the chemistry of the reaction accurately and couple the soot model to the main chemical reaction mechanism.

There exist a number of phenomenological soot models [12-15], which are able to predict number density and individual soot particle sizes. On the other hand these are computationally very expensive and require a significant amount of memory. The aim of the present work is not to compete in accuracy with these models but to create an engineering tool capable of predicting soot concentration with acceptable accuracy and low computational cost. It is also envisaged that via this engineering model efficient and novel pollutant abatement techniques are designed and optimized.

Widely accepted multiple step mechanisms for C/H/O systems [16] have been used in full or in reduced form to produce detailed combustion solution, which then have served as the basis for pollutant simulation: NO_x [17-18] or soot [19-22]**.** Most of the soot models employing this approach use a monodisperse soot size distribution, although this could be modified by adding a distribution function based on the spatial location [23], flame composition and temperature or a particle size fraction based on experimental observations [10]. The stochastic approach has also been a valid alternative to the simulation of soot particle size distribution [15, 24, 25].

Instead of defining a new, modified soot mechanism, the objective of the present work is the integration of a mathematical model able to perform soot predictions based on the eddy dissipation concept of Magnussen [3, 4, 26, 27] and that can be implemented in a commercial CFD solver.

A priori, the primary obstacle encountered to simultaneously reducing the soot and NO_x emissions is based on the fact that the main inhibiting thermodynamic property for soot - temperature - is a precursor - in exponential fashion - of NO_x. The work of Magnussen [5-7] proved both computationally and empirically the first order effect of small scale turbulence on reduction the emissions of soot.

Based on these results, the present work aims to demonstrate the qualitative trends in soot emissions when the flame is excited via three different pairs of harmonics with incommensurate periods, that is that the ratio of the periods is a non-integer number. The incommensurate pulse is generated with two sinusoidal pulses whose ratio of periods is a non-integer number. Equation 1 represents the generic expression of an incommensurate pair of frequencies where the secondary period has been multiplied by π, whereas equation 2 represents a typical harmonic function employed to create a simple sinusoidal profile at the fuel inlet.

$$u_{fuel} = 20.3 + A_1 \cos(2\pi\omega_1 t) + A_2 \cos(2\pi^2 \omega_2 t) \quad (1)$$

$$u_{fuel} = 20.3 + A \cdot \cos(2\pi\omega \cdot t) \quad (2)$$

Table 1 below contains boundary conditions and model specification for some representative flames simulated in this study.

Table 1

Flame	Frequency	A_1 (m/s)	A_2 (m/s)	ω_1 (1/s)	ω_2 (1/s)	$\bar{u}_{fuel}$ (m/s)
A	Incommensurate	0.5	0.5	100	100	20.3
B	Incommensurate	1.5	1.5	100	100	20.3
C	Incommensurate	2.5	2.5	100	100	20.3
D	Sinusoidal	5.52	-	100	-	20.3
p = 1atm, T_{fu} = 290K, T_{air} = 300K						

2. COMPUTATIONAL APPROACH

The simulation of a turbulent reacting jet requires the accurate resolution of the shear layer generated between the fuel and the oxidizer streams. Based on results from previous studies, the realizable k-ε was found to adapt well to this type of flow configuration, as it tackles some of the weaknesses observed in the standard k-ε, such as the normal stress becoming negative in highly strained flows, violation of the Schwartz inequality and also the round jet anomaly.

The diffusion flame simulated in the present work issues from a round nozzle of 4.11mm diameter, concentric to a larger nozzle from which flows a pilot flame in order to prevent lift and/or flame extinction. A two-dimensional quadrilateral grid with 216 nodes in the axial direction and 123 in the radial direction was employed to simulate the flame. Clustering of the nodes in the near region of the jet was applied in order to improve the accuracy of the simulation.

All transport equations were numerically approximated by application of a Second Order Upwind discretization method, where a control volume method is employed to convert the partial differential equations into algebraic expressions in order to obtain numerical results. With this approach in the CFD solver FLUENT, a higher order accuracy is achieved at cell faces through a Taylor series expansion of the cell-centred solution about the cell centroid. Governing equations are then integrated over the control volume to yield discrete equations that conserve each quantity on a control volume basis.

The chemistry model employed in these simulations is based on the solution of transport equations for species mass fractions. The reaction rates that appear as source terms in the species transport equations are computed from the Arrhenius rate expressions. In addition, and

in order to keep consistency with the soot model, the turbulence-chemistry interaction is accounted for through the eddy-dissipation model.

As shown in Table I, three incommensurate pulses were simulated, always with the same frequency value of 100Hz for both the primary and the secondary pulses; and also using equal amplitudes for both in all flame configurations tested.

Finally, in order to evaluate the advantages or disadvantages of using these types of pulses, a simple harmonic was defined such that the variance with respect to the time-averaged fuel inlet velocity was equivalent to that of flame C. Integrating the absolute value of the incommensurate signal over a long time span in order to minimize inaccuracies due to the non-periodicity did this. Then equalling the result to the integrated function of a simple harmonic with unknown amplitude over the same time interval, and finally solving for the unknown parameter.

The perturbations to the fuel inlet stream are aimed to enhance the mixing with the oxidizer stream by ultimately lengthening the mixing layer. As a result, this will increase the volume fraction of stoichiometric zones at the same time that the volume fraction of fuel rich zones, where soot forms, decreases. In addition, the fluctuations will transport oxygen from the oxidizer stream into the core of the reaction zone, thus aiding the soot burnout without the necessarily raising the flame temperature, consequently not increasing the NO_x emissions.

Thermal and prompt sources of NO_x have been considered in these simulations based on well established models [29-34, 37, 38]. In the case of thermal NO_x, the concentration of intermediate species OH and O are predicted as explained in references [37] and [38]. The NO_x model employed is described in detail in references [41] and [42].

3. THE SOOT MODEL

In a turbulent chemical reaction, there is a strong influence of the flow characteristics on the performance of the combustion process. As a result, an inhomogeneous structure of appearance of the reacting species will develop, linked to the inhomogeneous distribution of eddies in the flow. In these situations, the molecular mixing of the fuel and oxidant, which is highly intermittent, takes place inside the smallest-scale turbulence structures, referred to as the fine structures, and where the degree of mixing is comparable to that of a stirred reactor. These structures occupy only a fraction of the total volume of the domain and are believed to be three-dimensional vortex tubes or sheets of very small dimensions, comparable typically to the characteristic dimensions of the Kolmogorov microscales [28], which represent the last stage in the turbulent energy transfer cascade.

In general, turbulent flows of high Reynolds number present a spectrum of eddies of different sizes. These eddies transfer mechanical energy to their immediate neighbours and the interaction between the larger and the smaller eddies forms the main source of transfer and dissipation of turbulent kinetic energy (TKE). Finally, the dissipation of kinetic energy into heat, due to the work done by molecular forces on the eddies, takes place in these fine structures. Consequently, one of the major parameters that the model must solve for is the mass fraction of fine structures in the flow domain (γ^*), which is a function of the TKE and the turbulence dissipation rate (TDR), as given in equation 3 [4-7].

$$\gamma^* = 9.7 \cdot \left(\frac{\nu \cdot \varepsilon}{k^2} \right)^{0.75} \tag{3}$$

where k is the TKE, ν is the kinematic viscosity and ε is the TDR.

In addition to the prediction of the fraction occupied by the fine structures, it is essential to compute the mass transfer per unit mass and unit time between the fine structures and the surrounding fluid ($\dot{m}$) in order to evaluate the rate at which the fuel is mixed with the oxidant, as in equation 4, and, ultimately, the rate of fuel consumption.

$$\dot{m} = 23.6\left(\frac{\nu \cdot \varepsilon}{k^2}\right)^{0.25} \frac{\varepsilon}{k} \tag{4}$$

Because the reaction takes place within these fine structures and, consequently, the heat release, these will have a higher temperature than the mean temperature of the surrounding fluid. The increment of temperature (ΔT) with respect to the surrounding fluid is given by

$$\Delta T = \frac{\Delta H_R \cdot c_{min}}{\rho \cdot c_p} \tag{5}$$

where ΔH_R is the heat of reaction of the fuel, ρ is the density, c_p is the local specific heat capacity of the mixture and c_{min} is the minimum of c_{fu} and c_{o2}/r_{fu}, with c_{fu} and c_{o2} being the local gravimetric concentrations of fuel and oxygen respectively and r_{fu} is the stoichiometric oxygen requirement to burn 1kg of fuel.

The eddy dissipation model assumes local equilibrium between the fine structures and the surrounding fluid, hence the concentration of species in the fine structures and the surrounding fluid are related to the local mean concentrations by

$$\frac{c_i}{\rho} = \frac{c_i^*}{\rho^*}\gamma^*\chi + \frac{c_i^o}{\rho^o}\left(1 - \gamma^*\chi\right) \tag{6}$$

where χ is a local variable that accounts for the fraction of fine structures that are sufficiently heated to provoke combustion of the fuel. Super indices * and ^{o} refer to the fine structures and surrounding fluid respectively, and c_i is the local gravimetric concentration of species *i*.

The laminar soot model itself it based on the model developed by Tesner [8, 9], where the net formation of radicals from which soot forms -nuclei- and soot are computed with separate transport equations. The mean rates of nuclei and soot formatioin, according to this model, are given by equations 7 and 8, respectively.

$$R_{n,f} = n_o + (f - g)n - g_o N n \tag{7}$$

$$R_{s,f} = m_p(a - bN)n \tag{8}$$

Here, n_o is the spontaneous rate of nuclei formation, given by an Arrhenius type of expression, as per equation 9. The nuclei and soot concentration in particles/m^3 are denoted by *n* and *N*, respectively. The term (*f-g*) in equation 7 represents a model constant regarded as the nuclei branching-termination coefficient, in 1/s; whereas g_o is the nuclei coefficient of linear termination on soot, in m^3/part-s. In equation 8, *a* and *b* are model constants based on empirical investigation and the mass of a soot particle -m_p- is computed from the assumption that soot particles have spherical shape and that the density of these solid particles is of the order of 2 g/cm^3. In most combustion applications, these model constants do not require significant calibration, as these are based on simple reactions found in the reaction mechanisms of most hydrocarbon fuels.

$$n_o = a_o c_{fu} \exp(-E/RT) \tag{9}$$

In the expression for the spontaneous nuclei formation, equation 7, the activation temperature -E/R- is a model constant whose value holds for most combustion processes. The term a_o is a model constant throughout the simulation whose numerical value depends on the Reynolds number of the flame and must be stated accordingly. Likewise, the residence time will determine the size of the soot particles; thence the particle diameter will vary depending on the fuel inlet conditions and the flame characteristics. These two quantities are modified according to equations 10 and 11, where the fuel input and flame characteristics are introduced.

$$d_p = \frac{D \cdot c_{fu,o}^{1.6}}{U_o^{0.6}}\left(\frac{\rho_{fl}}{\rho_o}\right)\frac{1}{\nu_{fl}^{0.2}} \cdot const \tag{10}$$

$$\dot{m} \cdot a_o = const \tag{11}$$

where the sub-indices $_o$ and $_{fl}$ refer to inlet and flame conditions respectively, U is the axial fuel velocity and D is the diameter of the jet.

This soot model is then adapted within the context of the eddy dissipation theory by modifying the appropriate terms [5-7], as shown in equations 12 and 13, where Y_{nuc} and Y_{soot} are the mass fractions of nuclei and soot respectively.

$$R_{n,f} = \left(n_o^* \frac{\gamma^* \chi}{\rho^*} + n_o^o \frac{1-\gamma^* \chi}{\rho^o} + g_o n^* \frac{\gamma^* \chi}{\rho^*} \left(N^o - N^* \right) \right) \rho + (f-g) \rho Y_{nuc} - g_o \rho N^o Y_{nuc} \tag{12}$$

$$R_{s,f} = m_p \left(a \rho Y_{nuc} + b \rho N^* \frac{\gamma^* \chi}{\rho^*} \left(n^o - n^* \right) \right) - b n^o \rho Y_{soot} \tag{13}$$

The mean rates of soot and nuclei combustion -$R_{pollut,c}$- are comparable to the mean rate of fuel combustion -R_{fu}-, as shown in equations 14 and 15.

$$R_{pollut,c} = R_{fu} \frac{Y_{pollut}}{Y_{fu}} \tag{14}$$

where

$$R_{fu} = \dot{m} \cdot \chi \cdot c_{min} \tag{15}$$

The net rates of soot and nuclei formation are computed by subtracting the rates of combustion from the rates of formation, as per equation 16. The resulting expressions are then used as the source terms of two user-defined scalars, one for soot and the other one for nuclei, whose transport is simulated in a post-process fashion in the solver.

$$R_{pollut} = R_{pollut,f} - R_{pollut,c} \tag{16}$$

$$S = A + B\Phi \tag{17}$$

One of the major challenges encountered in the development of the subroutine was the appropriate selection of the linearization terms for the soot and nuclei transport equations. Source terms -S- used in the present study are written as a two-part variable, with well differentiated implicit and explicit parts, as shown in equation 17, where Φ is the dependent variable and A and $B\Phi$ are the explicit and implicit contributions respectively. The solver automatically determines whether the given linearization terms enhance the stability of the solver, and should this not be the case, the source terms are handled explicitly. In the present work it was found that the stability is significantly sensitive to the linearization terms, therefore careful algebraic manipulation of equations 12-17 were performed until the solver produced stable solution processes in all the cases studied.

4. RESULTS

The results presented in this work are intended to be the initial stage of an investigation into soot and NO_x emissions reduction in diesel automotive engines. The aim is to show that the emissions of these pollutants can be reduced simultaneously by means of pulsing the fuel jet. The techniques described here will later be adapted and applied to a piston-in-cylinder configuration in order to verify that similar conclusions can be drawn.

In CFD studies, it is common practice to perform an initial case study based on relatively simple laboratory conditions for which reliable experimental data is available. In the present work, the validation of the models concentrated on the simulation of a methane/air piloted diffusion flame. The fuel enters a 1.2m long cylindrical combustor at 20.3m/s through a round jet of 4mm diameter. The pressure is 1atm and the air velocity is negligible. The results showed reasonable

agreement with the experimental data [19, 20], taking into consideration that only a single-step reaction mechanism has been employed for the sake of simplicity and computational cost. Figure 1 depicts the radial flame temperature and mean mixture fraction and how they compare to the experimental measurements at a station located 350mm (x/D~86) downstream of the jet exit. Figures 2 and 3 depict the predicted soot volume fraction along vertical stations 350 and 425mm (x/D~104) downstream of the jet exit respectively. The results show reasonable agreement in the prediction of peak soot volume fraction, although the model predicts a much narrower distribution. In addition, it was also observed that stations at 375 (x/D~91) and 450mm (x/D~109) showed a better agreement with experiments, which can be interpreted as the rate kinetics and or jet mixing rate being lower in the model than in practice, thus causing the relative displacement of the computational results downstream of the experimental data. These drawbacks could be addressed by employing more refined turbulence modelling and reaction mechanism and also by a more comprehensive adjustment of the soot model. In the present case study, the primary objective was to find trends in the behaviour of soot and NO_x so that they can later be applied to more complex geometries; for that reason, a curve fit to reproduce already existing data was not performed.

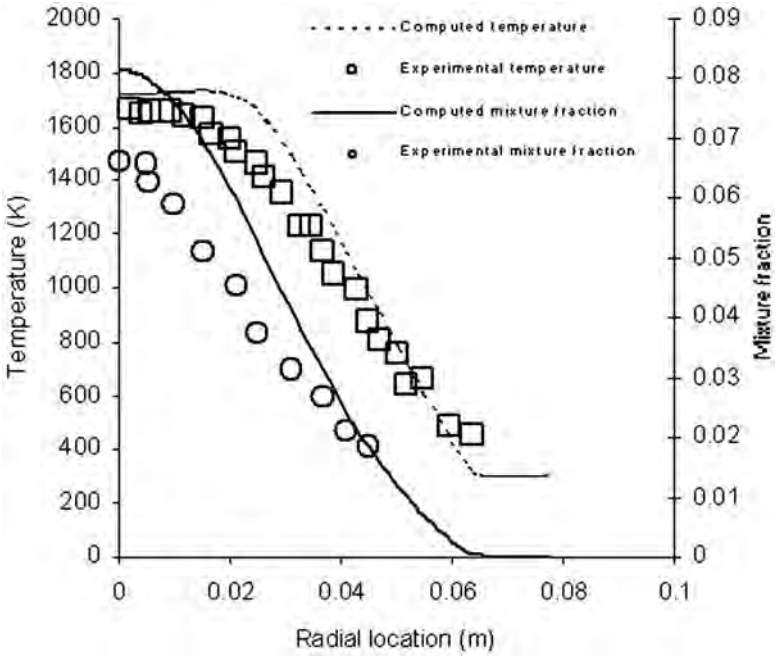

Fig. 1. Comparison between predictions and measurements of mean mixture fraction and temperature along radial station at x/D~86

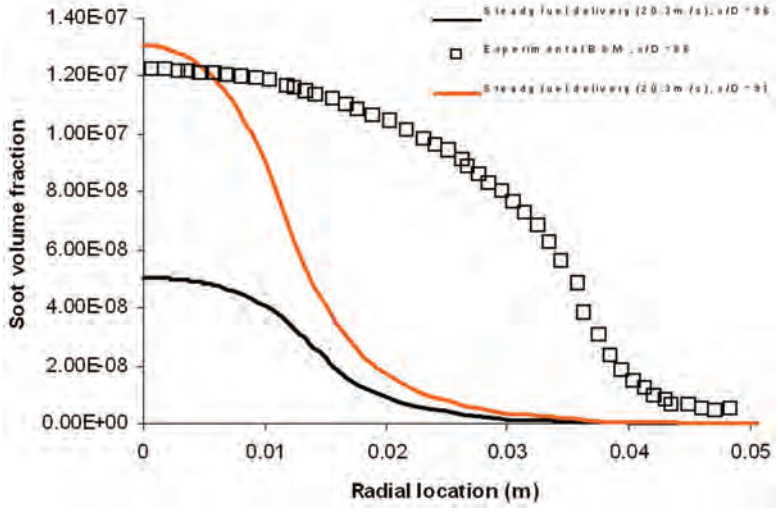

Fig. 2. Comparison between soot predictions and measurements along radial location at x/D~86

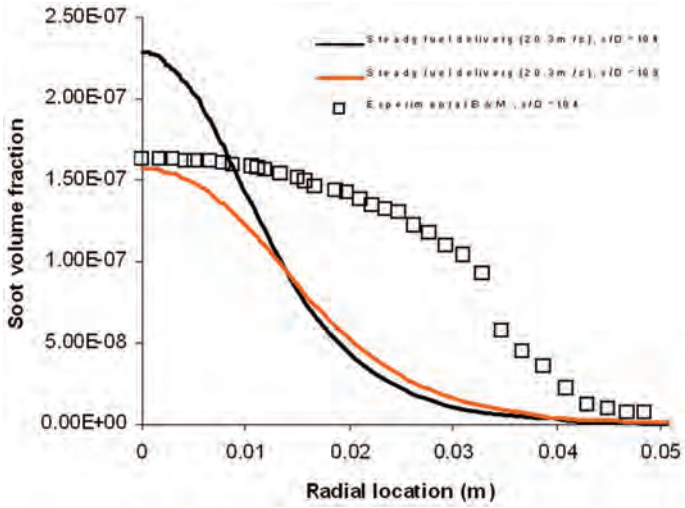

Fig. 3. Comparison between soot predictions and measurements along radial station at x/D~104

The use of incommensurate frequencies in non-linear systems generates a complex non-periodic fluctuation where a collection of different frequencies and amplitudes can be identified. The graph in figure 4 depicts the perturbation defined at the fuel inlet in the shape of instantaneous axial fuel inlet velocity for the three different amplitudes investigated. The Fast Fourier Transform -FFT- of this signal, depicted in figure 5, reinforced the premise that a spectrum of frequencies is generated.

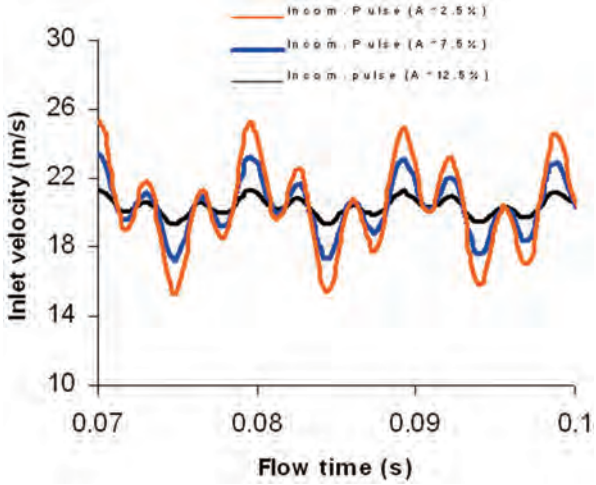

Fig. 4. Profile of incommensurate pulse as defined at the fuel inlet boundary for three different amplitudes

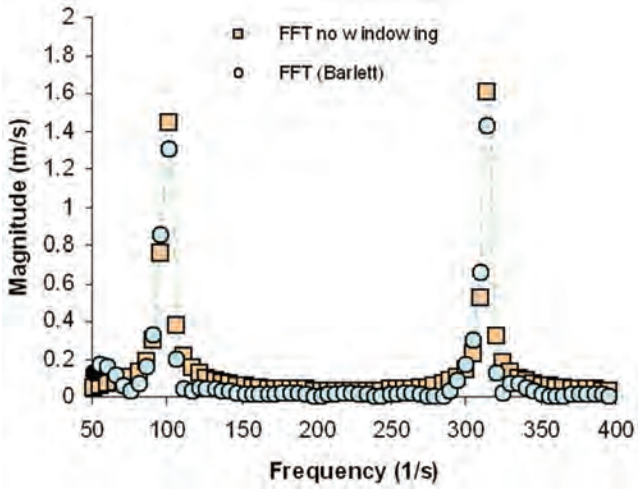

Fig. 5. Fast Fourier Transform of inlet fuel velocity with 7.5% pulse amplitude

A Fast Fourier Transform would ideally require data from a complete cycle, but given the non-periodicity of the incommensurate signal, a windowing function is applied in order to alleviate the discontinuities that would appear between the initial and the final points of the dataset employed to compute the FFT. The time history of both Strouhal number (eq. 18) and temperature at different locations within the shear layer are depicted in figure 6; and their corresponding FFT are depicted in figure 7. In the present work, the Strouhal number has been defined as the ratio between the input frequency (f_{inlet}) and the mixing frequency (ε/k). In the case of incommensurate frequencies, $f_{inlet} = 100\ (1 + \pi)$.

$$St = f_{inlet}\, k/\varepsilon \tag{18}$$

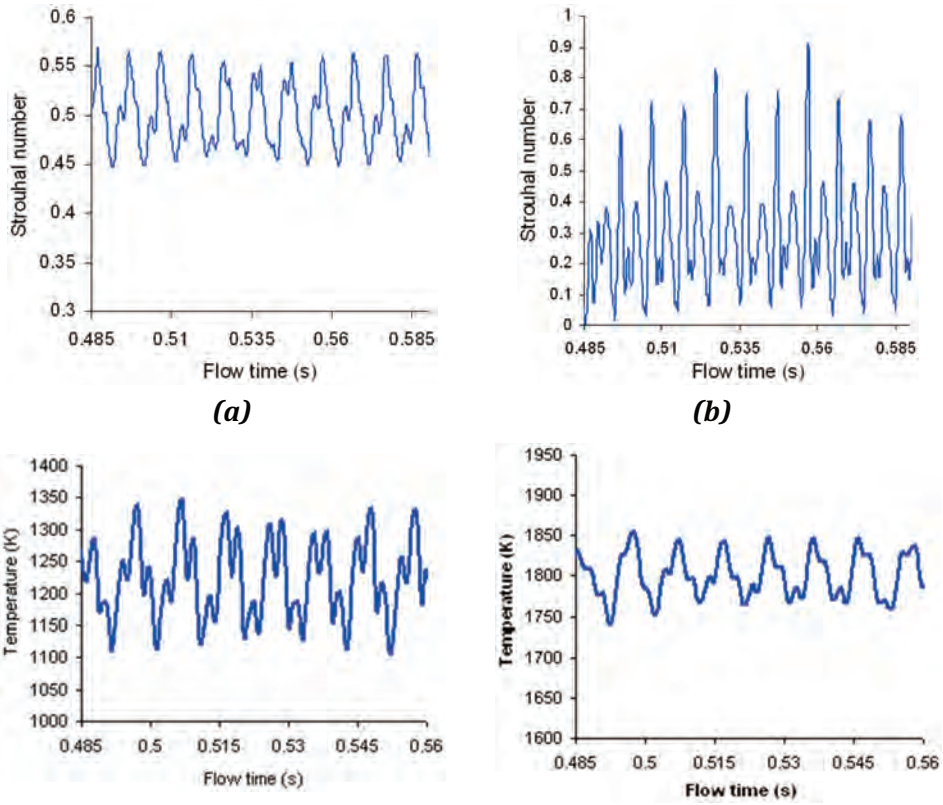

(a) *(b)* *(c)* *(d)*

Fig. 6. Time history of Strouhal number and temperature to incommensurate pulse at different locations –in mm: a) Strouhal number at (x,y) = (25, 5); b) Strouhal number at (x,y) = (25, 8); c) Temperature at (x,y) = (45, 5); d) Temperature at (x,y) = (50, 9)

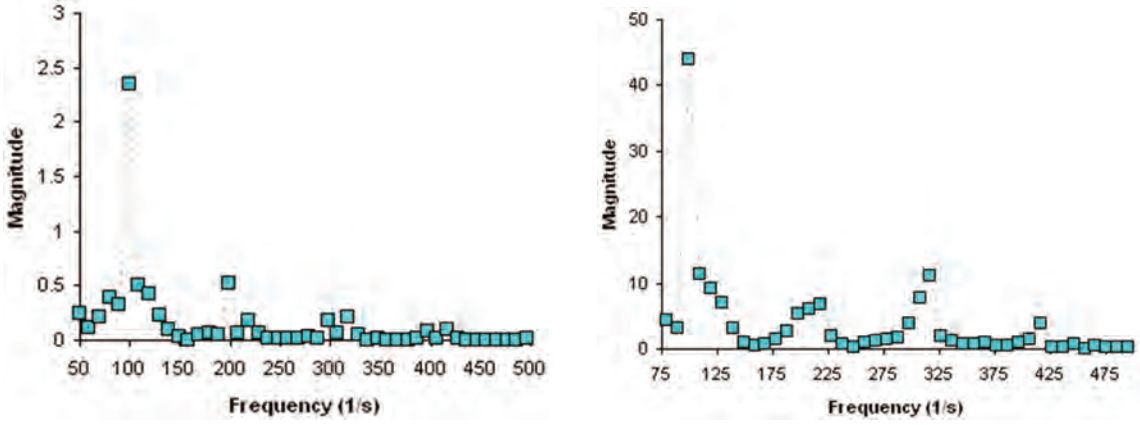

(a) *(b)*

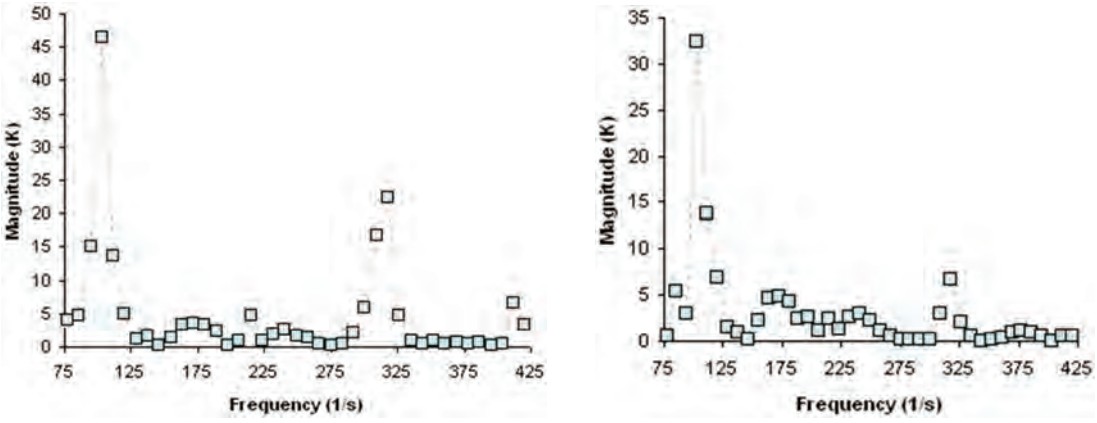

(c) *(d)*

Fig. 7. Fast Fourier Transform of mixing frequency and mean temperature at different locations: a) Strouhal number at (x,y) = (25, 5); b) Strouhal number at (x,y) = (25, 8); c) Temperature at (x,y) = (45, 5); d) Temperature at (x,y) = (50, 9)

Strong non-periodic fluctuations in the Strouhal number and temperature were observed in the near region of the jet and the FFT showed how the non-linear system responded to the incommensurate pulse by generating a range of induced perturbations. In addition, the value of the Strouhal number in flame D remained below orders of magnitude 10^{-1} up to downstream locations of x/D~35, as depicted in figure 8. On the contrary, higher Strouhal values were predicted in flame C, mainly due to the higher inlet perturbation frequency with respect to flame D. This would suggest that there is a noticeable coupling between the input frequency and the mixing frequency in this region of the flame, which comprises the zones where the majority of the mixing between fuel and oxidizer streams takes place.

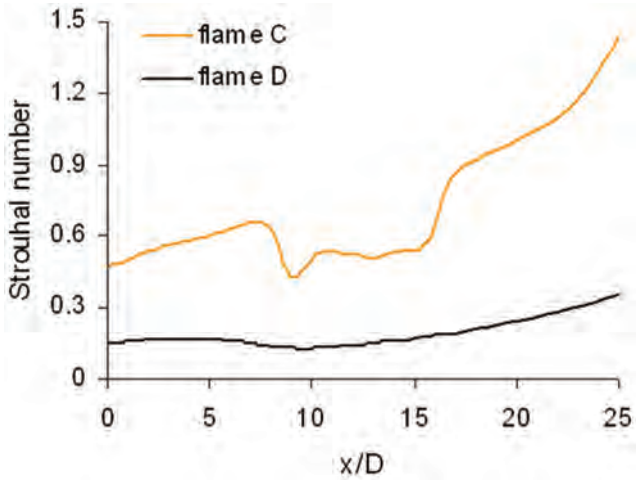

Fig. 8. Time-averaged Strouhal number along the axis of the flame

The profiles of the FFT display two primary peaks at 100 and 314 s^{-1}, which are the periods of the two frequencies enforced at the inlet, and also an additional spectrum of frequencies distributed among the primary one and of a smaller magnitude. When the FFT obtained in flame C and flame D are compared (figure 9), it is observed in both cases that the system generates a spectrum of frequencies. In figure 9, the amplitudes of the FFT in flame C are visibly lower than in flame C, probably due to the fact that the amplitude of the sinusoidal pulse is divided into the two parts of the incommensurate frequency.

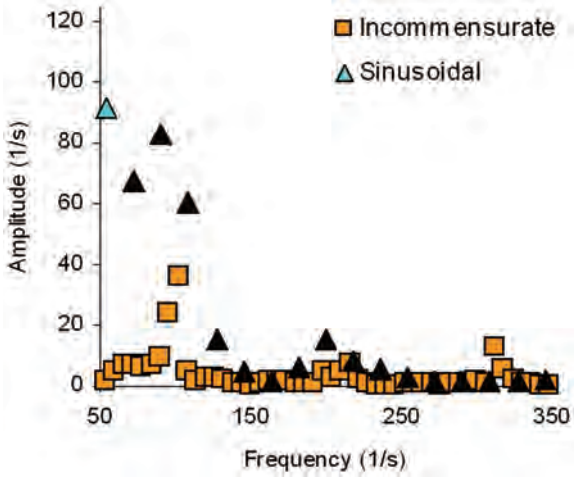

Fig. 9. Fast Fourier Transform of mixing frequency at (x,y)=(0.025,0.005) for flames C and D

Previous studies on the effects of fuel stream perturbations on pollutant emissions [39-42] have utilized similar feasible techniques to reduce soot and NO_x simultaneously in diffusion flames, albeit the characterization of the pulse was done mainly intuitively. On the other hand, the opposite effect is also possible: soot emissions can be enhanced by mainly employing perturbations with relatively long periods [43]. It is thus reasonable to believe that the pulse shape and sequencing would produce a significant effect on the soot emissions, and with the incommensurate pulse, the system is hoped it is likely to respond more actively to those frequencies similar to its resonance frequencies. Figure 10 depicts the computed soot volume fraction on the flame axis at x/D~86 for flames A, B, C and D, represented by the solid lines. The dotted lines represent the percentage reduction in soot volume fraction of the indicated excited flames with respect to the steady state predictions. Whereas the small perturbations observed in flame A implied small reductions is soot emissions -around 9%-, which could even be argued to reside within the margin of numerical error between computations, a more significant reduction was observed in flames B and C, when soot reductions of about 28 and 35% respectively were recorded.

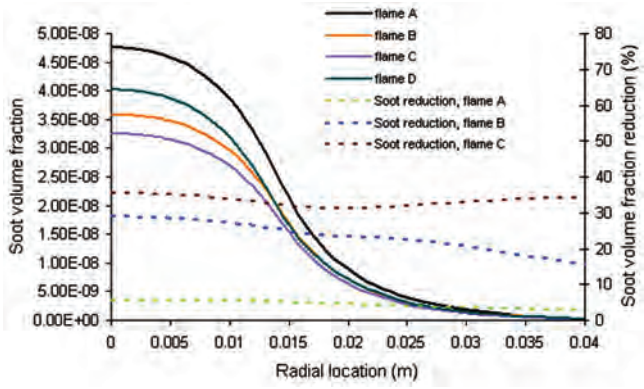

Fig. 10. Computed soot volume fraction and percentage reduction for incommensurate and harmonic perturbations along radial station at x/D~86

In all three cases, the percentage reduction remained relatively flat in the regions where peak soot concentrations were predicted. A very similar behaviour was also seen along the radial stations further downstream of the jet exit, as depicted in figures 11 and 12, which represent radial stations at x/D~91 and x/D~104.

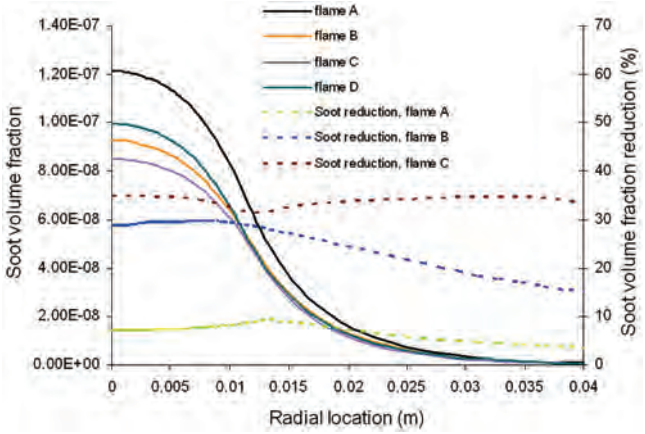

Fig. 11. Computed soot volume fraction and percentage reduction for incommensurate and harmonic perturbations along radial station at x/D~91

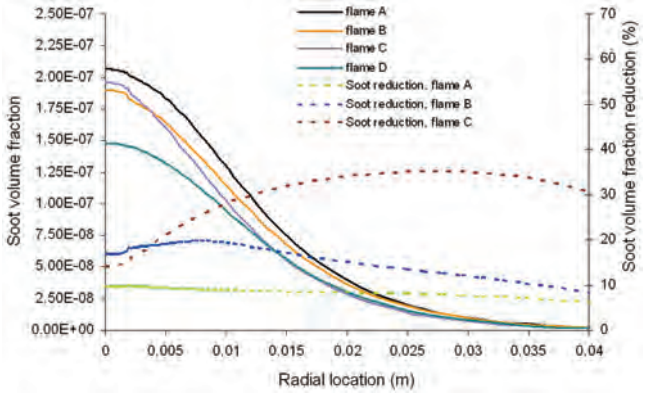

Fig. 12. Computed soot volume fraction and percentage reduction for incommensurate and harmonic perturbations along radial station at x/D~104

Despite the consistent reduction in soot emissions with increasing perturbation amplitude, it is reasonable to believe that the ratio between the percentage amplitude and the soot reduction must level or even decrease at some point. This behaviour is clearly depicted in figure 13, where the incommensurate pulse amplitude is plotted against the soot volume fraction reduction at three different axial locations.

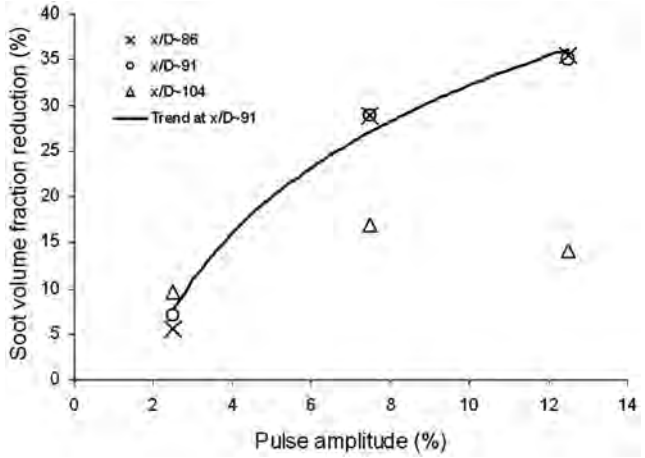

Fig. 13. Relationship between percentage amplitude of fuel stream perturbations and percentage gain in soot reduction

Although this study remains to be repeated with other fuels, a very similar pattern could be expected from other gaseous fuels, as long as the interaction between the fuel and oxidizer streams is comparable. If the soot predictions of flame C and D are compared, it can be appreciated that the along the two stations closer to the jet exit, x/D~86 and x/D~91, the former produces a more substantial decrease in soot emissions with respect to the steady flame than the sinusoidal pulse, as depicted in figures 10 and 11. On the contrary, the behaviour is reversed along stations further downstream, as seen in figure 12. Because of these dissimilarities, the axial soot volume fraction for the two pulses in question is compared, in order to enable a more accurate visualization of the soot distribution along the flame.

Figure 14 reveals a slight upstream displacement of the peak soot volume fraction of the sinusoidal pulse with respect to the incommensurate. More importantly, the maximum soot predicted in flame D is of the order of 12.5% lower than in flame C. Consequently, the use of incommensurate frequencies has not reported major benefits with respect to the simple sinusoidal pulse; however an extensive study should be performed in order to determine whether this is the norm with most of the composite incommensurate frequencies. On the other hand, the incommensurate frequency produces perturbations more often but less intense than the simple sinusoidal pulse. Consequently the depression caused by the non-periodic pulse is not as strong, thus not enforcing the oxidizer entrainment as much and also probably reducing the effective length of the mixing layer with respect to the simple sinusoidal pulse. In general, excited diffusion flames with periodic perturbations at the fuel inlet tend to create small regions of reacting flow very near the jet exit. As a result the flow temperature increases, enhancing the combustion reaction, which then shows a tendency to a pre-mixed behaviour. A comparison of the temperature and mixture fraction along the radial stations at x/D~91 and x/D~104 between the two excited flames is depicted in figures 15 and 16.

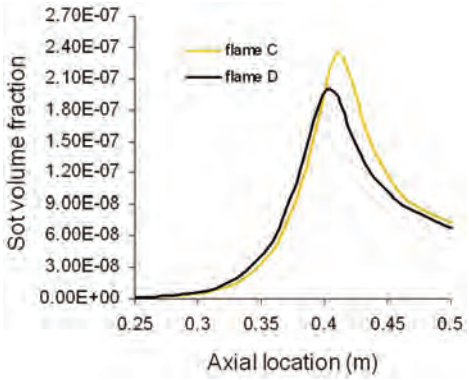

Fig. 14. Comparison of soot volume fraction along the axis of incommensurate and sinusoidal flames

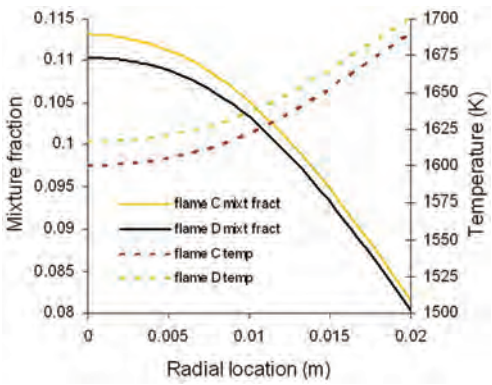

Fig. 15. Comparison of mean mixture fraction and flow temperature between the incommensurate and sinusoidal pulses at x/D~91

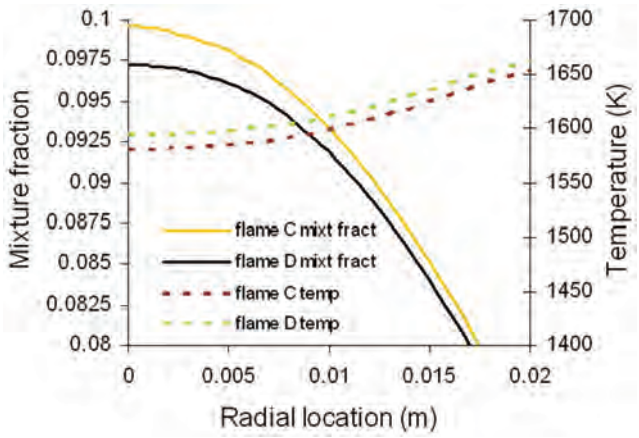

Fig. 16. Comparison of mean mixture fraction and flow temperature between the incommensurate and sinusoidal pulses at x/D~104

Despite small variations in the flow temperature and mixture fraction, these could be an indicator of lower soot volume fractions. In the case of NO_x the case is the opposite: the higher temperatures observed in flame D raise the amount of NO_x produced in the flame, as depicted in figures 17 and 18 for two of the radial stations. Unlike soot, NO_x is only dependent on the temperature, almost regardless of the turbulence intensity of the flow and can be safely considered to be a by-product without any interference with the main reaction.

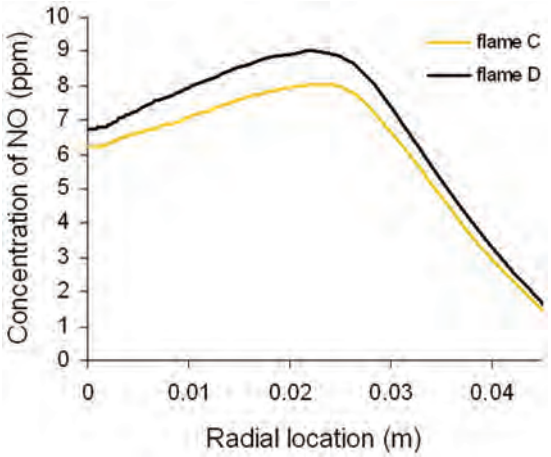

Fig. 17. NO concentration computed in sinusoida and incommensurate flames at x/D~86

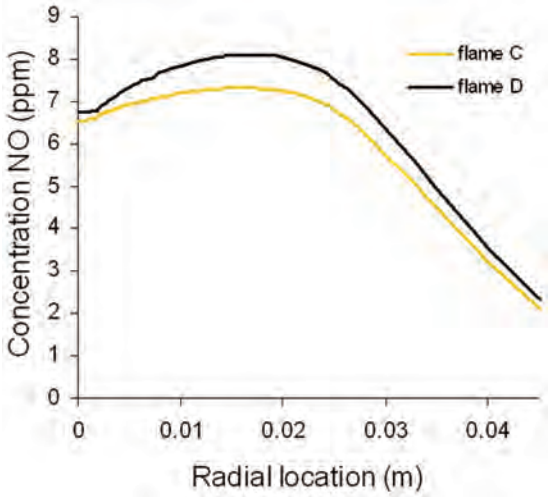

Fig. 18. NO concentration computed in sinusoidal and incommensurate flames at x/D~104

5. CONCLUSIONS

The present work has described and investigated a technique by which soot and NO_x emissions in a diffusion flame can be reduced simultaneously. This was achieved by enhancing the mixing of the fuel and oxidizer streams through a series of pulses in the fuel jet. The use of incommensurate pulses was intended to further enhance the mixing, although it caused a slight increment in the soot emissions with respect to its equivalent harmonic perturbation. On the other hand, it also generated lower flame temperatures, which reduced the NO_x emissions. It would then be a matter of evaluating which of the two pollutants, soot or NO_x, must be prioritized for emission reduction and select the type of perturbation accordingly. Nevertheless, it must be borne in mind that both techniques represent a significant reduction with respect to the steady flame.

REFERENCES

[1] Thilly, W.G. (1981) Soot Components as Genetic Hazards. In Lahaye. J and Prado, G (Eds.) Soot Combustion Systems and its Toxic Properties, Plenum Press, New York.pp. 1-12.

[2] Boyland, E. (1981) The Toxicology of Soot. In Lahaye, J. and Prado, G. (Eds) Soot Combustion Systems and its Toxic Properties, Plenum Press, New York. pp. 13-24.

[3] Magnussen, B.F. (1981) On the structure of turbulence and generalized eddy dissipation concept for chemical reaction in turbulent flow. 19th AIAA Science Meeting, St. Louis, Missouri, USA.

[4] Magnussen, B.F. (1989) Modelling of NO_x and soot formation by the eddy dissipation concept. International Flame Foundation First Topic Oriented Technical Meeting.

[5] Magnussen, B.F. (1974) An Investigation into the Behaviour of Soot in a Turbulent Free Jet C_2H_2-Flame. Proc. Combust. Instit., 15, 1415.

[6] Magnussen, B.F. and Hjertager, B.H. (1976) On Mathematical Modeling of Turbulent Combustion with Special Emphasis on Soot Formation and Combustion. Proc. Combust. Instit., 16, 719.

[7] Magnussen, B.F., Hjertager, B.H., Olsen, J.G. and Bhaduri, D (1979) Effect of Turbulence Structure and Local Concentrations on Soot Formation and Combustion in C_2H_2 Diffusion Flames. Proc. Combust. Instit. 17, 1383.

[8] Tesner, P.A., Snegiriova, T.D. and Knorre, V.G. (1971) Kinetics of Dispersed Carbon Formation, Combustion and Flame, 17, 253.

[9] Tesner, P.A. Tsygankova, E.I., Guilazetdinov, L.P., Zuyev, V.P. and Loshakova, G.V. The Formation of Soot from Aromatic Hydrocarbons in Diffusion Flames of Hydrocarbon-Hydrogen Mixtures. Combustion and Flame, 17, 279.

[10] Srivatsa, S.K. (1982) NASA-Lewis Research Center, NAS3-22542, NASA CR-167930, Garrett 21-4309.

[11] Khan, I.M. and Greeves, G. (1974) In Afgan, N.H. and Beer, J.M. (Eds) Heat Transfer and in flames, chapter 25. Scripta, Washington DC.

[12] Mauss, F., Schäfer, T., Bockhorn, H. and Rosner, D.E. (1994) Inception and Growth of Soot Particles in Dependence on the Surrounding Gas Phase. Combustion and Flame, 99, 697.

[13] Balthasar, M., Mauss, F., Knobel, A. and Kraft, M. (2002) Detailed Modeling of Soot Formation in a Partially Stirred Plug Flow Reactor. Combustion and Flame, 128, 395.

[14] Balthasar, M., Mauss, F. and Wang, H. (2002) A Computational Study of the Thermal Ionization of Soot Particles and Its Effect on Their Growth in Laminar Premixed Flames. Combustion and Flame, 129, 204.

[15] Balthasar, M. and Frenklach, M. (2005) Detailed Kinetic Modeling of Soot Aggregate Formation in Laminar Premixed Flames. Combustion and Flame, 140, 130.

[16] Warnatz, J. (1984) Rate Coefficients in the C/H/O System. In Gardiner Jr, W.C. (Ed.) Combustion Chemistry, Springer-Verlag, New York, Chap. 5. pp. 197-360.
[17] Fairweather, M., Woolley, R.M. (2004) First Order Conditional Moment Closure Modeling of Turbulent, Nonpremixed Methane Flames. Combustion and Flame, 138, 3.
[18] Fairweather, M. and Woolley, R.M. (2003) First Order Conditional Moment Closure Modeling of Turbulent, Nonpremixed Hydrogen Flames. Combustion and Flame, 133, 393.
[19] Brookes, S.J. and Moss, J.B. (1998) Measurements of Soot Production and Thermal Radiation from Confined Turbulent Jet Diffusion Flames of Methane. Combustion and Flame, 116, 49.
[20] Brookes, S.J. and Moss, J.B. (1999) Predictions of Soot and Thermal Radiation Properties in Confined Turbulent Jet Diffusion Flames. Combustion and Flame, 116, 486.
[21] Smooke, M.D., McEnally, C.S., Pferfferle, L.D., Hall, R.J. and Colket, M.B. (1999) Computational and Experimental Study of Soot Formation in a Coflow, Laminar Diffusion Flame. Combustion and Flame, 117, 117.
[22] Kronenburg, A., Bilger, R.W. and Kent, J.H. (2000) Modeling Soot Formation in Turbulent Methane-Air Jet Diffusion Flames. Combustion and Flame, 121, 24.
[23] Beltrame, A., Porshnev, P., Merchan-Merchan, W., Saveliev, A., Fridman, A., Kennedy, L.A., Petrova, O., Zhdanok, S., Amouri, F. and Charon, O. (2001) Soot and NO Formation in Methane-Oxygen Enriched Diffusion Flames. Combustion and Flame, 124, 295.
[24] Singh, J., Balthasar, M., Kraft, M. and Wagner, W. (2005) Stochastic Modeling of Soot Particle Size and Age Distributions in Laminar Premixed Flames. Proc. Combust. Instit. 30, 1457.
[25] Balthasar, M. and Kraft, M. (2003) A Stochastic Approach to Calculate the Particle Size Distribution Function of Soot Particles in Laminar Premixed Flames. Combustion and Flame, 133, 289.
[26] Chomiak, J. (1976) Dissipation Fluctuations and the Structure and Propagation of Turbulent Flames in Premixed Gases at High Reynolds Numbers. Proc. Combust. Instit. 16, 1665.
[27] Chomiak, J. (1972) Application of Chemiluminescence Measurement to the Study of Turbulent Flame Structure. Combustion and Flame, 18, 429.
[28] A.N. Kolmogorov, Journal of Fluid Mechanics, 13, 82, 1962.
[29] Blauwens, J., Smets, B. and Peeters, J. (1977) Mechanism of "Prompt" NO Formation in Hydrocarbon Flames. Proc. Combust. Instit. 16, 1055.
[30] Flower, W.L., Hanson, R.K. and Kruger, C.H. (1975) Kinetics of the Reaction of Nitric Oxide with Hydrogen. Proc. Combust. Instit. 15, 823.
[31] Monat, J.P., Hanson, R.K. and Kruger, C.H. (1979) Shock Tube Determination of the Rate Coefficient for the Reaction N_2+O->NO+N. Proc. Combust. Instit. 17, 543.
[32] Hanson, R.K. and Saliman, S. (1984) Survey of Rate Constants in the N/H/O System. In Gardiner W.C. (Ed), Combustion Chemistry, chap. 6. pp 361-462.
[33] Peters, N. and Donnerhack, S. (1981) Structure and Similarity of Nitric Oxide Production in Turbulent Diffusion Flames. Proc. Combust. Instit. 18, 33.
[34] Bilger, R.W. and Beck, R.E. (1975) Further Experiments on Turbulent Jet Diffusion Flames. Proc. Combust. Instit. 15, 541.
[35] Drake, M.C., Correa, S.M. Pitz, R.W., Shyy, W. and Fenimore, C.P. (1987) Superequilibrium and Thermal Nitric Oxide Production In Turbulent Diffusion Flames. Combustion and Flame. 69, 347.
[36] Warnatz, J. Lectures in NO_x formation in high temperature processes. University of Stuttgart, Germany.
[37] Fenimore, C.P. (1971) Proc. Combust. Instit. 13.
[38] De Soete, G.G. Overall Reaction Rates of NO and N_2 Formation from Fuel Nitrogen. Proc. Combust. Instit. 15, 1093.
[39] Lopez-Parra, F. and Turan, A. (2005) Computational Study on the Effect of Turbulence Intensity and Pulse Frequency in Soot Concentration in an Acetylene Diffusion Flame.

International Conference on Computational Sciences, pp.120-128, ICCS 2005, LCNS 3516, Springer-Verlag Berlin Heidelberg.
[40] Lopez-Parra, F. and Turan, A. (2005) Computational Study on the Effect of Pulse Characteristics on the Soot and NO_x Formation and Combustion in Diffusion Flames. Proceedings to the European Combustion Meeting. Louvain-la-Neuve, Belgium.
[41] Lopez-Parra, F. and Turan, A. (2005) Computational Study on the Effect of Turbulence Intensity in Soot Formation and Depletion in an Acetylene Diffusion Flame. Proceedings to the European Combustion Meeting. Louvain-la-Neuve, Belgium.
[42] Lopez-Parra, F. and Turan, A. (2005) Computational Study on the Effect of Turbulent Intensity and Pulse Frequency on Pollutant (Soot and NO_x) Concentration in an Acetylene Flame. Submitted for publication in Combustion and Flame.
[43] Bockhorn, H. Plenary lecture at European Combustion Meeting, The Combustion Institute, Louvain-la-Neuve, Belgium, 2005.

Fernando Lopez-Parra

OBLICZENIOWE BADANIE WPŁYWU INTENSYWNOŚCI TURBULENCJI I CZĘSTOŚCI PULSACJI NA EMISJĘ SADZY I TLENKÓW AZOTU NOX W DYFUZYJNYM PŁOMIENIU GAZOWYM

Streszczenie

Główny cel pracy przedstawionej w niniejszej publikacji dotyczy rozwoju i wdrażania cyfrowego modelowania i symulacji procesu tworzenia i zmniejszania wydzielania się sadzy w turbulentnym płomieniu dyfuzyjnym. Znaczenie takiego modelu opiera się na realizacji modelu będącego w stanie uwzględnić bezpośrednie skutki turbulencji na ilość sadzy wytwarzanej w uprzednio niezmieszanych płomieniach.

Istota tych badań skupia się na analizie osiowo-symetrycznych turbulentnych płomieni dyfuzyjnych spalania gazów: C2H2 i powietrza, wydobywających się z okrągłej dyszy o średnicy 3mm przy wartościach liczby Reynoldsa od 8000 do 16500. Ta tendencja zaobserwowana przy powstawaniu sadzy w zależności od intensywności turbulencji jest w zgodzie z wynikami empirycznymi z literatury, wskazującymi na zmniejszenie ilości powstawania sadzy wraz ze wzrostem turbulencji. Interakcja między składnikami i turbulencją była następnie wykorzystana w celu opracowania urządzenia, w którym zostałby osiągnięty cel równoczesnego obniżenia emisji sadzy i NOx.

Poziom turbulencji został zwiększony poprzez zastosowanie sinusoidalnej pulsacji do modulowania strumienia paliwa. Ta procedura zmniejsza wymiar obszaru bogatego w paliwo i podatnego na wydzielanie się sadzy poprzez wzrost wymieszania się paliwa i utleniacza.

Uzyskany model k-ε był wykorzystany do rozwiązania problemu turbulentnego transportu, natomiast symulację reakcji przeprowadzono z jednokrokowym mechanizmem reakcji, a współzależność turbulencji i reakcji chemicznych została rozwiązana za pomocą Wirowego Modelu Rozpraszania. Wielkość kroku obliczeniowego w pulsującym płomieniu wynosiła 1/20 okresu impulsu.

Model cząstek sadzy użyty w tej pracy uwzględniał dwa różne etapy procesu powstawania sadzy: etap powstawania jąder i etap wzrostu cząstek. W wyniku dwa rozwiązywane są dwa równania transportu − odpowiednio masy frakcji jąder i masy sadzy. Wdrożenie tego modelu odbywa się poprzez funkcje zdefiniowane przez użytkownika, zastępują one warunki źródłowe w domyślnych równaniach transportu sadzy. Ponadto, wytwarzanie NOx rozwiązano za pomocą klasycznego mechanizmu Zeldowicza z założeniem częściowej równowagi podczas wydzielania tlenu atomowego O i grup hydroksylowych OH.